In-situ investigation of the solidification dynamics in an irregular eutectic alloy

S Mohagheghi, S Bottin-Rousseau, M Şerefoğlu

In-situ investigation of the solidification dynamics in an irregular eutectic alloy

S Mohagheghi[1], **S Bottin-Rousseau**[2] **and M Şerefoğlu**[3]
[1] Istinye University, Department of Mechanical Engineering, Istanbul, Turkey
[2] Sorbonne Université, CNRS UMR 7588, Institut des NanoSciences de Paris, 4 Place Jussieu, 75252 Paris Cedex 05, France
[3] Marmara University, Department of Metallurgical and Materials Engineering, Maltepe, Istanbul, Turkey

Abstract. We present an in-situ experimental investigation of irregular eutectic growth dynamics observed optically in real time during directional solidification (DS) and rotating directional solidification (RDS) of a model transparent alloy, namely Amino-methyl-propanediol-Succinonitrile (AMPD-SCN). The SCN-rich solid grows with a nonfaceted solid-liquid interface, while AMPD forms thin whisker-like faceted crystals. With RDS, we observed simultaneously four distinct growth dynamics along the solidification front thanks to the rotation induced velocity ramp. At low velocity, AMPD crystals grow individually, with their leading tip ahead of – at a higher temperature than – the SCN-liquid interface which presents a linear undercooling change with V ramp. This regime is defined as a quasi-steady decoupled growth. During RDS, AMPD crystals are found to rotate with the sample in this regime. When they can reach the unsteady coupled-growth regime at higher V, since increasing V favors the formation of AMPD-SCN-liquid trijunctions, they start to branch noncrystallographically. At higher velocity, impurity effects lead to the formation of two-phase fingers. Further increase in the velocity results in the formation of primary SCN dendrites and a fine interdendritic eutectic microstructure. DS experiments confirmed the existence of those regimes at different velocities.

1. Introduction

Irregular eutectics are widely used in industry. In irregular eutectic alloys, at least one of the eutectic solid phases grows in a faceted way, and exhibits large, atomically smooth solid-liquid facets [1]. Many crystals of that kind grow on the shape of thin platelets (e.g., Si crystals [2]) or needles with "blocked" facets, the growth kinetics of which is highly nonlinearly dependent of the undercooling and is complexified by the role of crystal defects acting as elementary step flow sources. This entails nonsteady, irregular growth regimes, with a marked disorder in the solidified microstructures. Despite their practical importance, scientific studies on irregular eutectics remain essentially descriptive, and the simultaneous growth of faceted and nonfaceted crystals in an irregular eutectic alloy has been rarely addressed with the aim of highlighting the solidification processes that would not be specific to the chemistry of the alloy. In a recent paper [3], we showed that a faceted/nonfaceted transparent alloy, *i.e.* Amino-methyl-propanediol/Succinonitrile (AMPD-SCN) at near-eutectic concentration, can be used as an experimental model system for exploring the growth dynamics of irregular-eutectic microstructures in situ. As a main outcome, we identified a microstructural transition between decoupled- and coupled-growth as a function of the solidification velocity. Qualitative features that were thus revealed in a model

[3] Corresponding author

transparent system shed new light on previous observations in metallic irregular-eutectic alloys, such as austenite/graphite eutectic in cast irons [4, 5] and Ni-Ni_3Sn_4 alloy [6].
In this work, we present observations of the growth dynamics in thin AMPD-SCN samples during rotating directional solidification (RDS) experiments. During RDS, a thin sample is slowly rotated at constant angular velocities ω with respect to the axis of the fixed unidirectional temperature gradient G. Previously, the RDS method has been used to vary continuously the orientation of the crystals with respect to G during solidification [7-9]. Here, we took advantage of the imposed velocity ramp for the first time to study the different growth mechanisms observed as a function of growth velocity. As expected, the eutectic spacing is decreasing from center to the sample edge following the increase in velocity [8]. During RDS, the local V value increases from zero at the center of rotation to ωR at the sample edge in the lateral direction, x, where R (≈ 2.5 mm) is the outer radius of a circular sample. This *velocity ramp* along x, enabled us to observe different microstructures and to locate the transitions from one pattern to another in a sample with a given composition and geometry –and impurity content. Our RDS observations confirm the previously established classification into loosely separated categories: low-velocity patterns dominated by decoupled growth; intermediate velocity with transient coupling and noncrystallographic branching; high-velocity, impurity dominated regime with two-phase fingers. In addition, we observed a very high-velocity regime characterized by the formation of single-phase SCN dendrites with interdendritic eutectic. In this paper, we shall compare RDS and ordinary DS patterns, thus evidencing the efficiency of the RDS method at uncovering the complex V dependency of an irregular-eutectic growth dynamics.

2. Experimental procedure

Commercial AMPD and SCN were purified to prepare the eutectic alloy. The eutectic composition and temperature of the AMPD-SCN system are C_E = 97.39 mol% SCN and T_E = 325.7 K [10]. Thin glass-wall samples (with 12 µm nominal thickness) were filled by capillarity with the molten AMPD-SCN alloy under Argon atmosphere and sealed. Rectangular and both circular and rectangular samples were used for DS and RDS experiments, respectively. Samples were solidified with various pulling velocities (0.01 - 4 µm/s) during DS and angular velocities (0.015 and 0.032 °/s) during RDS. In RDS experiments, an average local velocity V_{ave} for each regime is reported since the pulling velocity linearly differs from one location to another. During RDS, solidification occurs in half of the sample while the other half undergoes directional melting – this region will not be shown in this paper, and we only focus on the region where solidification occurs. Additional information about RDS method can be found elsewhere [7, 11]. Similar to the DS experiments, the RDS stage was mounted on the XYZ stage of an optical microscope which is used in transmitted light mode for real-time observation of the solidification front.

3. Results and discussions

Using RDS experiments, we could observe four different types of growth dynamics at the solidification front, as shown Fig. 1. In these examples, the pulling velocity is linearly increasing from left (close to the center of rotation) to the right of the image (sample edge). Close to the center of rotation, where the velocity is low, in Fig. 1 (a), decoupled pattern forms in which AMPD crystals grow at higher temperatures than the SCN front. Coupled patterns, *i.e.* trijunctions where AMPD, SCN, and liquid are at local equilibrium, can be observed as going towards the right side of the image where the imposed velocity increases (Fig. 1 (a)). In addition, going from the left to the right side of this image, the increase in velocity results in a decrease of the AMPD apparent thickness and the distance between AMPD phases, yielding much finer solidification microstructure. The overall solid/liquid interface is highly tilted, compared to RDS experiments performed with regular eutectics [7], due to the fact that decoupled and coupled regimes are growing at different undercooling values (the decoupled regime is at higher temperatures than the coupled regime) which can be measured using Gz.
In an RDS experiment with larger sample, higher velocities are obtained close to the sample edge. The growth front towards the edge of this sample is shown in Fig. 1 (b). Towards the center of this sample,

only limited regions of decoupled and coupled growth dynamics are observed due to the high velocity gradient. At this high V_{ave} regime shown in Fig. 1 (b), two-phase fingers and primary SCN dendrites with interdendritic eutectic were observed. Two-phase fingers in this system are composed of a thin AMPD crystal surrounded by dendritic SCN phase. Two-phase fingers were observed during univariant growth of a non-faceted binary alloy in the presence of a small quantity of a third compound or a foreign impurity [12]. We suspect that the trace of a third compound may remain a few ppm. SCN dendrites with interdendritic eutectic is an expected observation when the system is not at the coupled zone as defined by Kurz and collaborators [13]. Evolution of this structure from two-phase fingers occurs when the velocity increases and, as a result, primary SCN dendrites grow at a higher temperature than the fine interdendritic AMPD – SCN coupled eutectic. From the left to right of the image, although V increases, the temperature of the solidification front with two-phase finger structure does not change much. However, when the transition from the two-phase finger to the primary dendrites with interdendritic eutectic occurs, the tips of the primary dendrites grow at higher temperatures, and the solidification front of the interdendritic eutectic structure is at lower one than the two-phase fingers front temperature. After the transition, the tips of the primary dendrites are growing almost at the same temperature although the velocity increases (Fig. 1 (b)). On the other hand, the overall solidification front temperature of the interdendritic eutectic decreases as V increases, as expected. Primary SCN dendrites shown in the right side of Fig. 1 (b) originate from a single grain as their orientation is identical.

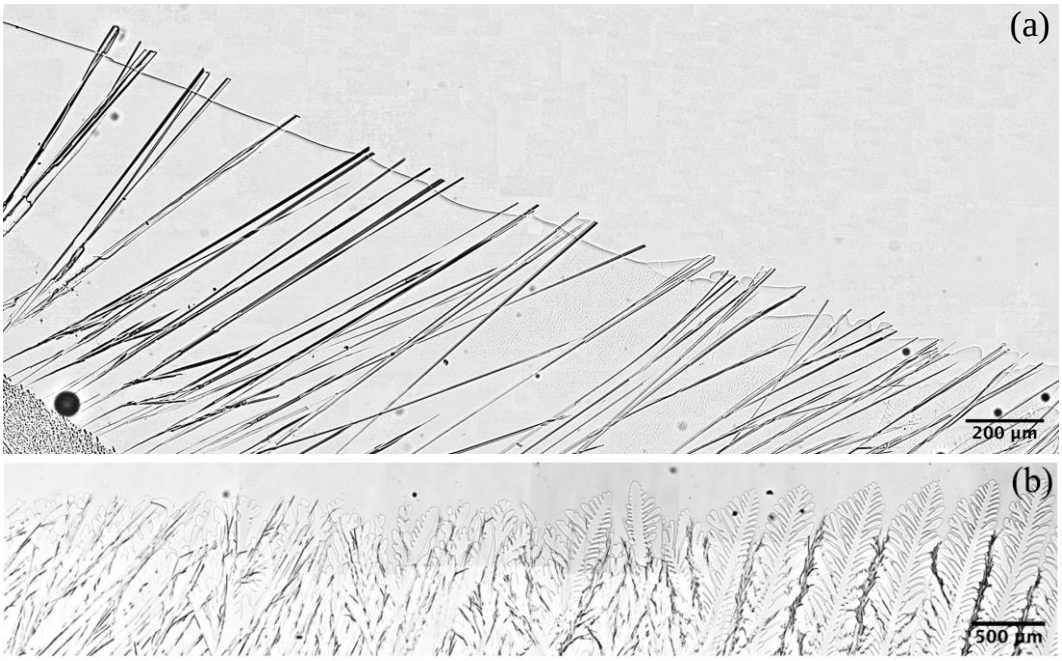

Figure 1. RDS images showing four different types of growth dynamics at the solidification front. As the imposed velocity increases from left to the right side of the images: (a) Transition from decoupled to coupled. $\omega = 0.032^{o}/s$, G = 5.1K/mm, $0 < V_{ave} < 1.3\mu m/s$. (b) Transition from two-phase fingers to primary SCN dendrites with interdendritic eutectic structure. $\omega = 0.015\ ^{o}/s$, $1.6 < V_{ave} < 3.9\ \mu m/s$.

In the decoupled regime, the faceted phase cannot branch either crystallographically or noncrystallographically. Therefore, further rotation of the sample is accompanied by the rotation of the faceted crystals with the sample. The example shown in Fig. 2 (a) perfectly illustrates the strict rotation of growing faceted crystals for 108° with the sample without branching. It is the extreme case similar to the locked interphases observed in regular eutectics that were studied using RDS stages [9,11]. Absence of both branching and thickening of the crystal indicate that the overall growth direction of the faceted AMPD is in the normal direction of the facet plane at the tip of the crystal in the decoupled regime. When the tip of the crystal shown with the arrow in Fig. 2 (a) reached a higher V regime (due to growing

towards the edge of the sample), coupling occurs. At this moment, the AMPD crystal branches noncrystallographically, as shown by the arrow in Fig. 2 (b). In the coupled regime, the AMPD crystals either continue to rotate with the sample or branch noncrystallographically.

The results of RDS experiments can be confirmed using DS experiments performed at different pulling velocities (Fig. 3). At low velocities, say $V < 0.3$ μm/s, the solidification front comprises a few faceted needle-like AMPD crystals growing mostly ahead of the planar nonfaceted SCN/L interface (Fig. 3 (a)). Therefore, trijunctions, where the growing interfaces of the two solids meet the liquid, are absent, *i.e.* the AMPD-SCN-liquid contact is not at local equilibrium. The tilting angles of AMPD crystals are inherited from the crystallographic orientations in the as-cast solid.

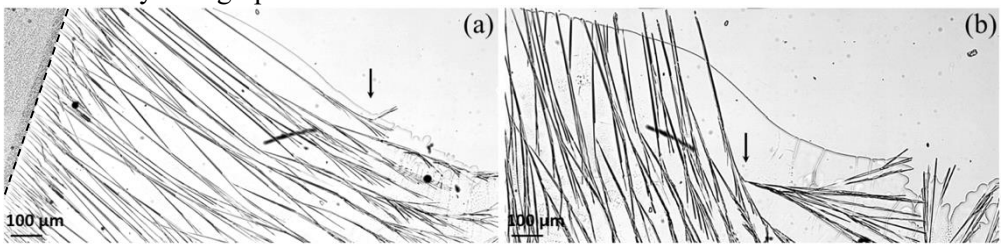

Figure 2. RDS images taken at two different rotation angles, (a) $\Delta\theta = 108°$, (b) $\Delta\theta = 150°$. In this experiment, the initial solid/liquid interface (dashed-line in (a)) was perpendicular to the growth direction at $\theta = 0°$. $\omega = 0.026°/s$, $G = 5.1$ K/mm, $0 < V_{ave} < 0.6$ μm/s. The arrows show the same AMPD crystal.

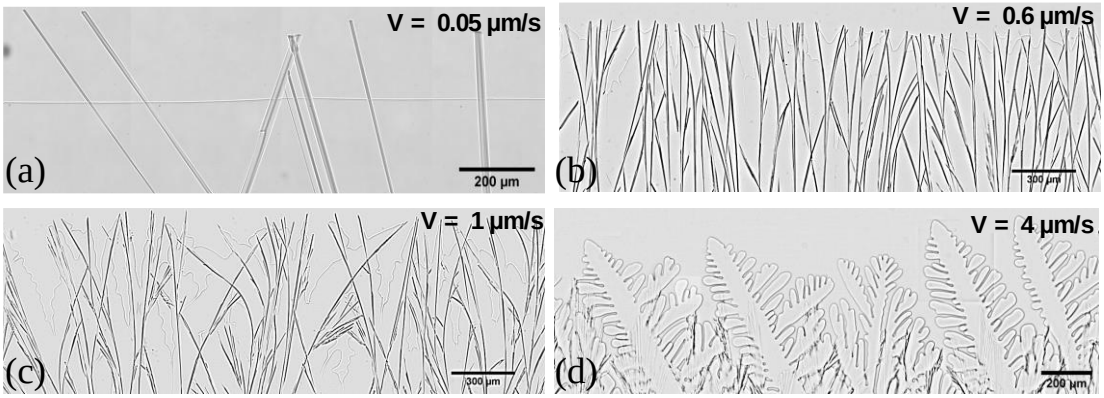

Figure 3. DS images showing four different types of growth dynamics, namely (a) Decoupled at V = 0.05 μm/s, (b) Coupled at V = 0.6 μm/s, (c) Two-phase fingers at V = 1 μm/s, and (d) Primary dendrite with interdendritic eutectic at V = 4 μm/s. For (a) – (c) G = 7.5 K/mm, for (d) G = 8.5 K/mm.

When the velocity is between $0.3 < V \leq 0.6$ μm/s, unsteady coupled growth is observed (Fig. 3 (b)). In this pattern, many trijunctions form between SCN, AMPD, and liquid phases at the solidification front; however, these trijunctions are frequently pinning and depinning indicating unsteadiness in the growth dynamics. The dynamics was complexified by a phenomenon that is not commonly observed in nonfaceted systems, which was called noncrystallographic branching in reference to spherulitic growth [14]. During noncrystallographic branching, the faceted crystal, in contrast to lamellar and rod splitting in regular eutectics, forms a new crystal with a small misorientation with respect to the parent phase. These frequent branching events lead to a dramatic increase in the number of AMPD crystals and hence reducing the AMPD interphase spacing as shown in Fig. 3 (b).

At high velocity regime ($0.6 < V < 3$ μm/s), two-phase fingers form (Fig. 3 (c)). It is well-established that two-phase fingers form due to impurities in the alloy, as a result of which SCN/L interface is nonplanar and most of the time dendritic. Some of the fingers shown in Fig. 3 (c) are oriented in the

direction of the temperature gradient and some are highly inclined. The inclined blocked AMPD facets that are not exposed to the liquid impose the growth direction, indicating the strong role of the anisotropy of SCN/AMPD interphase boundary. The tip of the interior AMPD crystal can be coupled with the SCN dendrite tip, *i.e.* forming a temporary trijunction. In this case, the blocked facets at the sides of the AMPD crystal are not exposed to the liquid and the two-phase finger can continue to grow for a long time. However, if such a coupled growth configuration is broken and the blocked facets of the AMPD crystal are exposed to liquid, new crystals can be created by noncrystallographic branching from the parent AMPD crystal as shown in Fig. 4. Interestingly, these branching events can occur both at the tip and at locations far away from the tip of the AMPD crystal as shown in Fig. 4 (b) and (d), respectively. At even higher velocities, primary SCN dendrites with interdendritic eutectic structure are observed (Fig. 3 (d)). Using RDS experiments we already showed that both planar and nonplanar SCN growth microstructures can be observed along the same solidification front. To clarify this point further, we performed another experiment where two major downward velocity jumps were performed. First, the sample was grown at V = 4 μm/s and the resulting microstructure was composed of primary dendrites with interdendritic eutectic. Then, the first downward V jump was employed from 4 μm/s to 1 μm/s. During the transient, the distance between the primary SCN dendrite tips and the eutectic decreased with time. In about 10 minutes, two-phase fingers were established. At the tip of the two-phase fingers, SCN and AMPD grow roughly at the same temperature. After 635 seconds, the second downward V jump was employed from 1 μm/s to 0.1 μm/s. During this second transient, many AMPD crystals were eliminated, SCN/L interface became planar, and the growing tips of the AMPD crystals were ahead of the SCN/L interface. At the end, decoupled microstructure at V = 0.1 μm/s was established after an overnight experiment. Observation of decoupled microstructure where SCN/L is essentially planar after solidifying primary SCN dendrites proves that the transitions between all these four regimes are only due to velocity. It is important to note here that the threshold velocities from the two-phase fingers to the primary dendrites with interdendritic eutectic structure would depend on the impurity level.

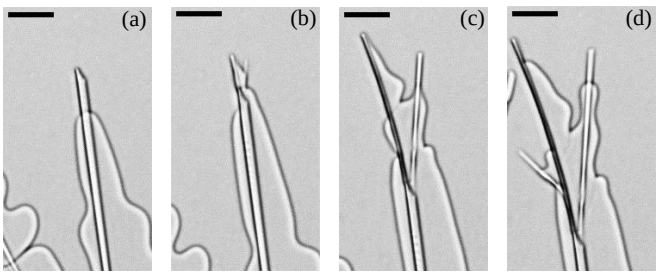

Figure 4. Time sequence showing noncrystallographic branching events of a two-phase finger (a) t = 0, (b) t = 78 s, (c) t = 180 s, (d) t = 234 s. Noncrystallographic branchings occur at the growing tip of AMPD and from the side facet of the same crystal. V = 1 μm/s, G = 7.5 K/mm. The scale bar is 50 μm.

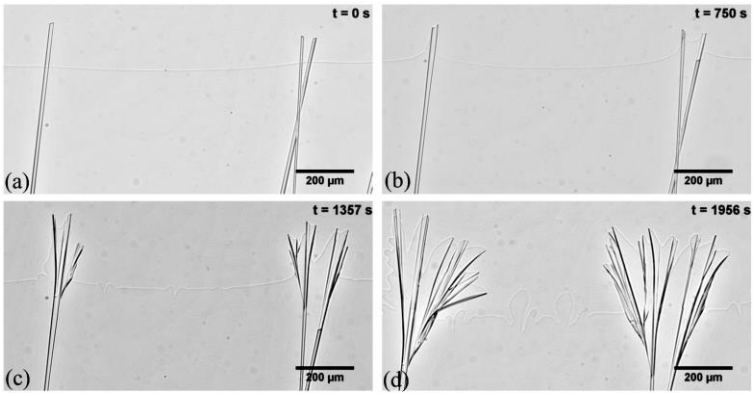

Figure 5. Evolution of the solidification front from decoupled to coupled pattern upon upward V-jump from 0.1 to 0.5 μm/s. G = 7.5 K/mm.

An upward velocity jump experiment was also performed to study the dynamics of the decoupled to coupled transition. After the establishment of the decoupled regime at V = 0.1 μm/s, an upward velocity jump to 0.5 μm/s was applied**,** and the time is taken as reference, t = 0. As shown in Fig. 5 (a), there are only three crystals in the observation window. As expected from decoupled pattern, the SCN/L interface is planar, and all the crystals grow at higher temperatures than SCN solidification front. After the velocity jump to V = 0.5 μm/s, the SCN close to the AMPD crystals grow faster along the blocked facets of the AMPD crystals which results in a shallow depression at the SCN/L interface between the far away crystal and the two close crystals. Due to this forward jump of SCN, AMPD/SCN/L trijunctions are formed as shown in Fig. 5 (b). At this point, the condition for noncrystallographic branching is satisfied and frequent branching events result in creation of many thin AMPD fibers growing in a coupled manner with SCN (Fig. 5 (c) & (d)). Due to the continuous noncrystallographic branching events, slightly-misoriented branches form over time. As a result of the cumulative effect of these misorientations, new crystals with more than 60° misorientation with respect to the parent phase are observed in Fig. 5 (d).

Summary and Conclusions

We used a model organic transparent alloy system and in-situ observations to investigate the growth dynamics of irregular eutectic alloys. V-ramp imposed by the RDS experiments enabled us to further investigate the various microstructures obtained at different velocities during DS experiments [3] at the same solidification front. Observing all the three previously reported microstructures at the same solidification front confirms that for a given alloy composition, both the microstructure and the growth dynamics, i.e. being coupled vs. decoupled etc., are selected only by the growth velocity. Furthermore, at the very high-V regime, i.e. towards the edge of the sample during RDS experiments, we observed that the system gets out of the coupled-zone region, which results in observation of primary SCN dendrites with eutectic at the interdendritic region. As a result, irregular eutectic growth dynamics can be classified into four main categories as: *(i) Decoupled growth* is mainly observed at low-velocity regime where a steady-state decoupled growth pattern is likely to exist, but its stability is limited by nonlinear interfacial kinetics at the growing tips of the faceted crystal. *(ii) Unsteady coupled growth* is observed at the intermediate velocity regime along with frequent noncrystallographic branching and elimination events. Over long experiments, a balance is reached between the branching and elimination of the AMPD crystals. Hence, the average eutectic spacing is essentially constant. *(iii) Growth of two-phase fingers* is observed at high-velocity regime. Noncrystallographic branching events yield disordered solidification microstructure. *(iv) Growth of primary SCN dendrites with interdendritic eutectic* is observed at even higher velocities. Increase in the velocity drives the system out of the coupled-zone region and favors the formation of primary SCN phase with dendritic interface. The eutectic structure evidently grows at a lower temperature than the tip of the dendritic SCN and in between the dendrites. Unsteady coupled growth with noncrystallographic branching events is observed in the interdendritic eutectic region. The transitions between these growth regimes are reproducible and reversible. Locating a sharp V threshold for these transitions seems to be not feasible. We show the use of RDS stage clearly evidences the V-dependency of the growth dynamics and the selection of the microstructure. By performing RDS experiments, we were able to observe all four patterns in a sample at the same solidification front where the composition and impurity content are constant. Additionally, the RDS results demonstrate the locking dynamics of the AMPD crystals with rotation in the decoupled regime. When reaching the coupled regime, AMPD crystals either continue to rotate or branch noncrystallographically through formation of a triple junction.

The current observations of faceted/nonfaceted eutectic microstructures can assist in explaining some mechanisms of pattern formation in industrial irregular alloy systems. Further theoretical and numerical developments as well as further detailed experimental studies are needed to fully explain the growth dynamics of irregular eutectics.

Acknowledgments
We are deeply grateful to S. Akamatsu for enlightening discussions and to our late colleague G. Faivre for sharing with us his profound thinking at the beginning of this work. This work is funded by TÜBİTAK 2509 (Grant no: 217M089) and Campus France (PHC BOSPHORUS 39706RE).

References

1. Fisher DJ, Kurz W 1980 *Acta Metallurgica* **28** 777-94
2. Hellawell A 1970 *Progress in Materials Science* **15** 3-78
3. Mohagheghi S, Bottin-Rousseau S, Akamatsu S, Şerefoğlu M 2020 *Scripta Materialia* **189** 11-5
4. Lacaze J, Sertucha J 2018 *China Foundry* **15** 457-63
5. Mohagheghi S, Bottin-Rousseau S, Akamatsu S, Şerefoğlu M, Lacaze J 2021 The 12th International Symposium on the Science and Processing of Cast Iron, 9-12 November, Muroran city in Hokkaido, Japan, 40-41
6. Hou N, Belyakov SA, Pay L, Sugiyama A, Yasuda H, Gourlay CM 2018 *Acta Materialia* **149** 119-31
7. Akamatsu S, Bottin-Rousseau S, Şerefoğlu M, Faivre G 2012 *Acta Materialia* **60** 3206-14
8. Mohagheghi S, Şerefoğlu M 2019 *Metallurgical and Materials Transactions A* **50** 5221-33
9. Mohagheghi S, Şerefoğlu M 2018 *Acta Materialia* **151** 432-42
10. Witusiewicz VT, Sturz L, Hecht U, Rex S 2005 *Acta Materialia* **53** 173-83
11. Akamatsu S, Bottin-Rousseau S, Şerefoğlu M, Faivre G 2012 *Acta Materialia* **60** 3199-205
12. Akamatsu S, Faivre G 2000 *Physical Review E* **61** 3757-70
13. Kurz W, Fisher DJ 1979 *International Metals Reviews* **24** 177-204
14. Bisault J, Ryschenkow G, Faivre G 1991 *Journal of Crystal Growth* **110** 889-909